NUMERICAL ANALYSIS OF AN ACOUSTIC LEAKY WAVE ANTENNA FOR UNDERWATER APPLICATIONS

Alejandro Fernández-Garrido

Department of Information and Communications Technologies, Universidad Politécnica de Cartagena, 30202 Cartagena, Spain.
alejandro.fernandez3@upct.es

Rubén Picó

Institut d'Investigació per a la Gestió Integrada de les Zones Costaneres (IGIC), Universitat Politècnica de València (UPV), 46730 Gandia, València, Spain.
rpico@upv.edu.es

María Campo-Valera

Telecommunication Research Institute (TELMA), Universidad de Málaga, 29010 Málaga, Spain.
maria.campo@ic.uma.es

Abstract. Numerical simulations in COMSOL Multiphysics are used to investigate the behavior of an Acoustic Leaky Wave Antenna (ALWA) operating in an underwater environment. The model characterizes both the propagation of elastic waves within the antenna structure and their coupling with the surrounding fluid by integrating the *Pressure Acoustics* and *Solid Mechanics* modules in a fully coupled multiphysics framework. Key acoustic parameters such as radiation patterns, transmission and reflection coefficients, radiation efficiency and directivity are evaluated. The results demonstrate the effectiveness of COMSOL in accurately modeling complex acoustic-structural interactions and support the potential of ALWAs for underwater directional sound applications.

I. INTRODUCTION

Acoustic Leaky Wave Antennas (ALWAs) are structures that can direct sound in different orientations by allowing part of the wave to leak out of a waveguide as it travels [1, 2]. This direction depends on the frequency of the sound, enabling beam steering without electronics.

Originally developed for electromagnetic waves [3–5], this concept has been adapted to acoustics using specially designed materials called metamaterials [6]. In air, these designs have shown that sound can be directed forward or backward by adjusting frequency [7–9].

Underwater applications are more complex due to stronger interactions between the waveguide and the fluid [10, 11]. Recent advances use elastic materials with internal resonators to overcome this challenge and steer beams underwater [12].These antennas offer a compact, passive alternative for sonar, communication, and sensing, with performance controlled by structure rather than electronics [13].

In this context, the present work employs COMSOL Multiphysics to simulate the full geometry of an ALWA [14]. The model incorporates elastic wave propagation within the antenna structure and its coupling with the surrounding fluid domain. Using the Pressure Acoustics and Structural Mechanics modules in a fully coupled multiphysics environment, the study evaluates key performance metrics including the radiation pattern, reflection and transmission coefficients, radiation efficiency, and directivity. The results provide a comprehensive assessment of the antenna's acoustic behavior and demonstrate the feasibility of using using these antennas for frequency-dependent beam steering in subsea applications.

II. THEORY

This section provides the theoretical framework for the antenna design.

To support the simulation presented later, this section summarizes the theoretical basis of ALWAs. These structures incorporate periodic openings along a waveg-

uide that enable part of the guided wave to leak into the surrounding medium, producing directional radiation [15]. As shown in *Figure 1*, the radiated energy follows a defined angle θ_r, determined by the waveguide's propagation constants.

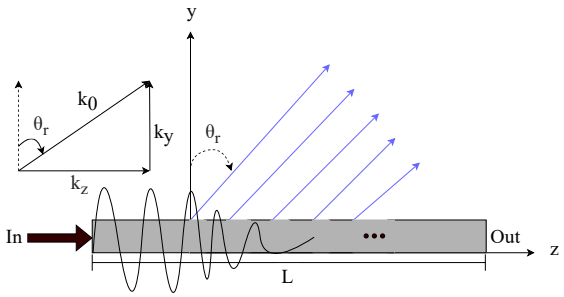

Figure 1: Illustration of an ALWA structure composed of a waveguide aligned along the z-axis with radiating openings. The diagonal blue lines represent emitted acoustic beams.

The radiated pressure field near the antenna is given by:

$$P(z,y) = p_0\, e^{-j\,k_y\,y} e^{-j\,k_z\,z} e^{j\omega t}, \tag{1}$$

where $k_z = \beta - j\alpha$ defines propagation along the waveguide and radiation losses, and $k_y = \sqrt{k_0^2 - \beta^2}$ governs behavior in the transverse direction [15, 16]. Radiation occurs when $\beta < k_0$, with the radiation angle given by:

$$\theta_r = \sin^{-1}\left(\frac{\beta}{k_0}\right) \tag{2}$$

The beamwidth at half-power can be approximated as:

$$\Delta\theta \approx \frac{\lambda}{L\cos(\theta_r)} \tag{3}$$

Due to the dispersive nature of β, the radiation angle θ_r varies with frequency, enabling frequency-based beam steering [4, 15].

III. MATERIALS AND METHODS

This section presents a detailed description of the simulation process based on the finite element method (FEM), including the modules employed, the problem geometry, the selected materials, the meshing process and the analysis performed.

A. Modules

The simulation was carried out using the commercial software *COMSOL Multiphysics*® 6.3, employing the *Acoustics* and *Structural Mechanics* modules modules [17].

The Acoustics module: uses the *Pressure Acoustics, Frequency Domain* interface, which solves the Helmholtz equation in the frequency domain to model the propagation of acoustic waves in quiescent fluids. This linear formulation treats acoustic pressure as a scalar field and supports the modeling of attenuation using homogenized fluid models, including porous media and thermo-viscous losses. The interface also allows for the definition of incident fields and localized sources, such as monopoles and dipoles.

Mathematically, the interface solves the Helmholtz equation in the frequency domain for prescribed excitation frequencies, and it also supports eigenfrequency and modal analyses.

The Structural Mechanics module: employs the *Solid Mechanics* interface using a 2D axisymmetric formulation, well-suited for problems exhibiting rotational symmetry. This interface is based on Navier's equations of linear elasticity and enables the computation of displacements, stresses, and strains in solid domains. The axisymmetric approach reduces computational complexity while preserving the essential physical behavior. Additional capabilities, such as contact modeling and nonreflecting boundaries, can be accessed when extended modules are included.

B. Geometry

The simulated antenna consists of an array of adjacent unit cells. As shown in *Figure 2*, each unit cell is composed of two solid steel waveguides (dark grey) located at each end, together with a lead ring (light grey) that acts as a leakage element. Inside this leakage element is a steel membrane (yellow), supported by two lead rings inside an air-filled cavity.

The designed acoustic antenna is composed of a waveguide of cylindrical geometry and axial periodicity, formed by a series of axisymmetric unit cells. Each cell includes a steel waveguide with an outer radius r_wg and an axial length L_{wg}. Inside, a radial cavity lead (shunt) characterized by a radius r_{sh} and a thickness t_{sh}, which allows the introduction of local resonances necessary for obtaining negative dynamic modulus, is

incorporated. In addition, each cell contains a disk-shaped steel mass, defined by a height h_m and a radius r_m, mounted at the center by means of elastic elements.

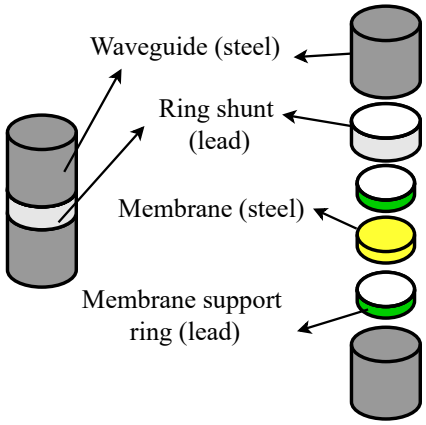

Figure 2: Parts of a unit cell that make up the proposed antenna.

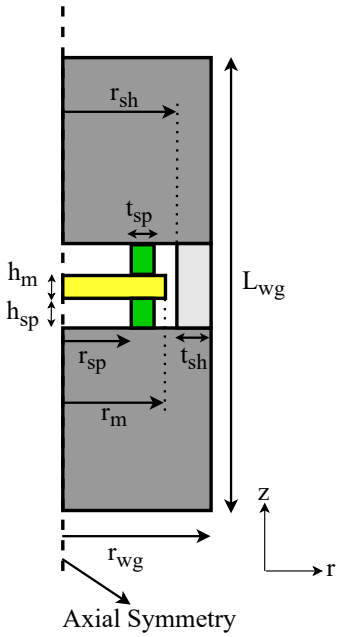

Figure 3: Schematic representation of a unit cell with geometric parameters.

Figure 3 provides a schematic representation of the unit cell, indicating the dimensional parameters associated with each structural element.

These supporting elements are modeled as lead spring-like rings with inner radius r_{sp}, radial thickness t_{sp}, and axial height h_{sp}. Together, these components act as a mass-spring system tailored to induce negative dynamic density within the unit cell. The full geometry preserves rotational symmetry about the longitudinal axis of the waveguide, which is advantageous for both fabrication and numerical simulation via axisymmetric finite element models. The complete antenna comprises N identical unit cells, resulting in a total physical length of $N \cdot L_{wg}$. This length has been designed to ensure that the propagating elastic waves are adequately attenuated, through radiation leakage and material damping before reach the antenna, thus minimizing unwanted reflections.

The specific numerical values of all geometric parameters are provided in Table 1.

Variable	Description	Value
r_{wg}	Radius of the unit cell	49.6 mm
L_{wg}	Length of the unit cell	72.7 mm
r_{sh}	Radius of the leakage	41.6 mm
t_{sh}	Thickness of the leakage ring	7.9 mm
r_{sp}	Radius of the ring supporting the membrane	37.1 mm
t_{sp}	Thickness of the membrane support ring	3.1 mm
h_{sp}	Separation between membrane and waveguide	8.7 mm
h_m	Thickness of the membrane	12.2 mm
r_m	Radius of the membrane	40.3 mm
N	Number of cells	40

Table 1: Geometric parameters of the proposed antenna.

C. Materials

The ALWA is composed of multiple homogeneous, isotropic elastic materials selected to achieve a balance between mechanical functionality, manufacturability, and acoustic performance. The main structural component, the cylindrical waveguide, is fabricated from steel, chosen for its high stiffness and density, which enable efficient transmission of elastic waves while maintaining structural integrity under dynamic loading. The mass element, which acts as the inertial

core in the mass-spring system, is also made of steel to preserve material continuity and ensure sufficient mass contrast with the elastic support elements.

The spring-like supports and the shunt (leaky) cavity are constructed from lead, a softer and denser metal with a significantly lower Young's modulus compared to steel. This contrast in stiffness is essential for enabling localized elastic deformation, which contributes to the emergence of negative dynamic effective parameters. Lead's high density also aids in enhancing the dynamic interaction with the surrounding fluid, promoting acoustic radiation. The values of the material properties are listed in the Table 2.

Variable	Description	Value
ρ_{Pb}	Density of lead	$11\,340\,\mathrm{kg/m^3}$
E_{Pb}	Young's module of lead	$16.3\,\mathrm{GPa}$
ν_{Pb}	Poisson's ratio of lead	0.44
ρ_{Steel}	Density of steel	$7850\,\mathrm{kg/m^3}$
E_{steel}	Young's module of steel	$200\,\mathrm{GPa}$
ν_{steel}	Poisson's ratio of steel	0.3
c	Speed of sound of seawater	$1500\,\mathrm{m/s}$
ρ	Density of seawater	$1027\,\mathrm{kg/m^3}$

Table 2: Material properties of the proposed antenna.

D. Physical Characterization of the Model

COMSOL Multiphysics distinguishes between domain conditions, boundary conditions and point conditions within each physical interface. [17]. The present study employs the physics of *Pressure Acoustics, Frequency Domain*; and *Solid Mechanics*. *Multiphysics* coupling is used to model the interaction between the elastic structure and the surrounding fluid.

1. Pressure Acoustics, Frequency Domain

Boundary conditions: In the physics of *Pressure Acoustics, Frequency Domain*, the **Port** condition was applied to excite the antenna, enabling the analysis of acoustic wave behavior in the marine environment. This condition models the input and output ports of the antenna, located at the ends of the corresponding waveguides. The governing equation is:

$$p_t = \sum_{i \in bnd} A^{in} e^{i\phi}(s_{ij} + \delta_{ij}) p_i \tag{4}$$

when the summation over i is taken over all ports on the given boundary bnd, and s_{ij} is the scattering parameter. A^{in} is the amplitude of the incident field at port j, ϕ is the phase of the incident field, and p_i denotes the mode shape of the i-th port. The port type used is circular, with the radial mode number set to zero (m=0).

At the boundary of the external medium, a **Perfectly Matched Boundary (PMB)** condition was applied. This condition functions as a Perfectly Matched Layer (PML), effectively absorbing outgoing waves at open boundaries without requiring the explicit definition of a separate layer in the geometry. The PML formulation is automatically implemented using COMSOL Multiphysics' extra dimension feature. Since the simulation is carried out in water, the PML scaling factor was adjusted from its default value of 1 to 5, in order to enhance absorption efficiency under underwater conditions.

Finally, the **Exterior Field Calculation** condition has been used to calculate the far-field antenna radiation pattern. The equations that model it are:

$$p_{\text{ext}}(R) = -\frac{1}{4\pi} \int_{S(r)} e^{ik\frac{r\cdot R}{|R|}} \left(\nabla p(r) - ikp(r)\frac{R}{|R|} \right) \cdot (-\mathbf{n})\, dS \tag{5}$$

$$p_{ext} = \lim_{R \to \infty} p(R) \tag{6}$$

In Equation (5), the term $p_{\text{ext}}(R)$ represents the acoustic pressure at a far-field observation point R. The prefactor $\frac{1}{4\pi}$ corresponds to the normalization constant derived from the free-space Green's function in three-dimensional acoustics. The integration is performed over a closed surface $S(r)$ that encloses the radiating source.

The exponential term $e^{ik\frac{r\cdot R}{|R|}}$ represents an outgoing spherical wave, which approximates a plane wave in the far-field direction defined by the unit vector $\frac{R}{|R|}$. Here, k is the acoustic wavenumber, defined as $k = \frac{2\pi}{\lambda}$, with λ being the wavelength.

The term $\nabla p(r)$ is the spatial gradient of the acoustic pressure evaluated at a point r on the integration surface. $p(r)$ denotes the acoustic pressure itself at that point. The dot product with $-\mathbf{n}$, where $\mathbf{n}$ is the outward-pointing normal vector to the surface, accounts for the projection of the acoustic field onto the surface's normal direction. Finally, dS represents the differential surface element.

Equation (6) defines the far-field acoustic pressure p_{ext} as the limit of the pressure field $p(R)$ when the observation point R tends toward infinity. This expression is used to formally characterize the pressure radiated into the far-field region.

The *Figure 4* reflects where these boundary conditions have been applied

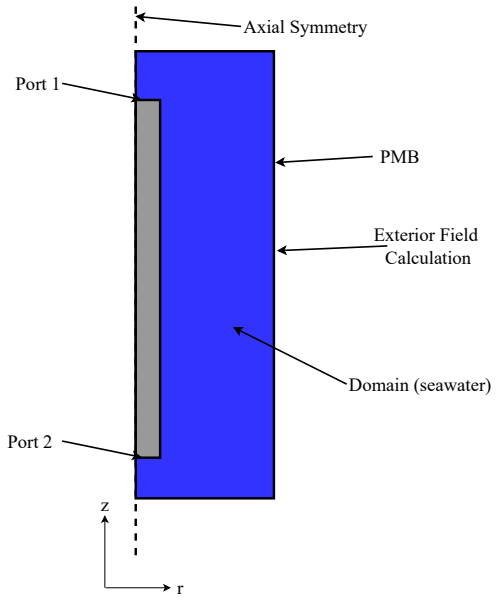

Figure 4: ALWA boundary conditions with Pressure Acoustics module

2. Solid Mechanics

Domain conditions: Used in the physic *Solid Mechanics*, only one has been used, that of **Linear Elastic Material**, but with different characteristics, one for lead and the other for steel.

The **Linear Elastic Material** domain condition is used to define the elastic behavior of solids under the assumption of linear stress-strain relationships. This setting applies to the entire volume of a domain and allows the user to specify material symmetry (isotropic, orthotropic, or anisotropic) along with two independent elastic constants, such as Young's modulus and Poisson's ratio. These parameters are essential for constructing the stiffness matrix that governs the mechanical response. Additionally, the material density can be included for dynamic simulations or to account for volumetric forces like gravity. For nearly incompressible materials, a mixed formulation can be enabled, introducing pressure as an additional dependent variable to improve numerical stability. The model can be further enriched by adding subfeatures such as thermal expansion, damping, initial stress, or viscoelasticity. Overall, this domain setting forms the foundation for accurately capturing the linear elastic response within the simulation.

The mechanical response of a linearly elastic solid, including various inelastic effects, is described by the following field equations and constitutive relationships. The balance of linear momentum in the frequency domain is expressed as:

$$-\rho\omega^2\mathbf{u} = \nabla\cdot\mathbf{S} + \mathbf{F}^v e^{i\phi} \tag{7}$$

Here, ρ is the mass density, ω is the angular frequency, $\mathbf{u}$ is the displacement field, $\mathbf{S}$ is the total stress tensor, and $\mathbf{F}^v e^{i\phi}$ represents a harmonic volume force.

Under axisymmetric assumptions, the displacement vector simplifies to:

$$\mathbf{u}(R,\Phi,Z) \rightarrow (u,0,w)^T \tag{8}$$

The total stress is decomposed into elastic and inelastic components as follows:

$$\mathbf{S} = \mathbf{S}_{\text{inel}} + \mathbf{S}_{\text{el}}, \quad \boldsymbol{\epsilon}_{\text{el}} = \boldsymbol{\epsilon} - \boldsymbol{\epsilon}_{\text{inel}} \tag{9}$$

The inelastic strain tensor incorporates various physical effects and is given by:

$$\boldsymbol{\epsilon}_{\text{inel}} = \boldsymbol{\epsilon}_0 + \boldsymbol{\epsilon}_{\text{ext}} + \boldsymbol{\epsilon}_{\text{th}} + \boldsymbol{\epsilon}_{\text{hs}} + \boldsymbol{\epsilon}_{\text{pl}} + \boldsymbol{\epsilon}_{\text{cr}} + \boldsymbol{\epsilon}_{\text{vp}} + \boldsymbol{\epsilon}_{\text{ve}} \tag{10}$$

Here, the subscripts denote: initial (ϵ_0), externally induced (ϵ_{ext}), thermal (ϵ_{th}), hygro-swelling (ϵ_{hs}), plastic (ϵ_{pl}), creep (ϵ_{cr}), viscoplastic (ϵ_{vp}), and viscoelastic (ϵ_{ve}) strains.

The elastic stress is related to the elastic strain through the linear constitutive equation:

$$\mathbf{S}_{\text{el}} = \mathbf{C} : \boldsymbol{\epsilon}_{\text{el}} \tag{11}$$

The inelastic part of the stress may contain additional terms, such as initial and external pre-stresses:

$$\mathbf{S}_{\text{inel}} = \mathbf{S}_0 + \mathbf{S}_{\text{ext}} + \mathbf{S}_q \tag{12}$$

The total infinitesimal strain tensor is defined as the symmetric part of the displacement gradient:

$$\boldsymbol{\epsilon} = \frac{1}{2}\left[(\nabla \mathbf{u})^T + \nabla \mathbf{u}\right] \tag{13}$$

Finally, the elasticity tensor $\mathbf{C}$ is a function of the material properties, typically the Young's modulus E and Poisson's ratio ν:

$$\mathbf{C} = \mathbf{C}(E, \nu) \tag{14}$$

These expressions together form the basis for modeling the mechanical behavior of solids with both elastic and inelastic effects in frequency-domain simulations.

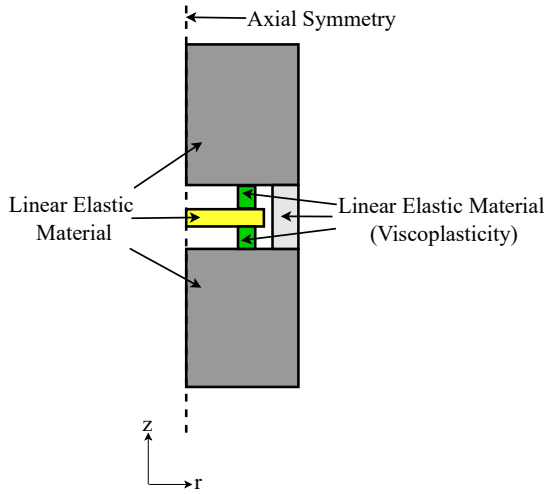

Figure 5: ALWA boundary conditions with Solid Mechanic module

3. Multiphysics

In the context of multiphysics simulations involving fluid-structure interaction, COMSOL Multiphysics provides the **Acoustic-Structure Boundary** condition to accurately couple an acoustic pressure field with the structural motion of a solid boundary. This boundary condition enforces continuity of the normal component of momentum and ensures that the pressure loading on the structure is dynamically consistent with the acceleration of the boundary. Specifically, it enables bidirectional coupling between the acoustic pressure in the fluid domain and the structural displacement in the solid domain, which is essential in applications such as vibroacoustics, ultrasonic transducers, and aeroelasticity.

The governing relations for this coupling, as implemented in COMSOL, are described below. These equations express both the balance of normal forces at the boundary and the pressure-induced aerodynamic force acting on the structure.

At the exterior interface between the acoustic medium and the structure, the normal component of the acoustic momentum flux is balanced by the structural acceleration:

$$-\mathbf{n} \cdot \left(\frac{1}{\rho_c}\left(\nabla p_t - \mathbf{q}_d\right)\right) = -\mathbf{n} \cdot \mathbf{u}_{tt} \tag{15}$$

Here, $\mathbf{n}$ is the unit normal vector pointing out of the fluid domain, ρ_c is the compressible fluid density, p_t is the total pressure, and $\mathbf{q}_d$ is a damping or additional momentum flux vector. The term $\mathbf{u}_{tt}$ represents the second time derivative of the structural displacement, i.e., the acceleration of the boundary.

The resulting aerodynamic force applied on the structure is given by:

$$\mathbf{F}_A = p_t \mathbf{n} \tag{16}$$

In cases where the structure is surrounded by fluid on both sides (such as a panel with upper and lower surfaces in contact with different fluid domains), the interface condition must be enforced on both surfaces:

$$-\mathbf{n} \cdot \left(\frac{1}{\rho_c}\left(\nabla p_t - \mathbf{q}_d\right)\right)_{\text{up}} = -\mathbf{n} \cdot \mathbf{u}_{tt} \tag{17}$$

$$-\mathbf{n} \cdot \left(\frac{1}{\rho_c}\left(\nabla p_t - \mathbf{q}_d\right)\right)_{\text{down}} = -\mathbf{n} \cdot \mathbf{u}_{tt} \tag{18}$$

The net aerodynamic force acting across the structure, due to the pressure difference between the lower and upper fluid domains, is:

$$\mathbf{F}_A = p_{t\text{down}} \mathbf{n} - p_{t\text{up}} \mathbf{n} \tag{19}$$

These conditions ensure a consistent and physically accurate interaction between the pressure field in the fluid and the motion of the structure. They are crucial for capturing the correct dynamic behavior of systems involving acoustic excitation and structural response.

E. Mesh

The finite element mesh was generated using a user-controlled strategy in COMSOL Multiphysics to accurately capture the elastic-acoustic coupling present in the underwater leaky wave antenna. A *Free Triangular* meshing approach was adopted to conform to the axisymmetric geometry of the unit cell, particularly in regions with complex features such as the *shunt cavity* and the mass-spring inclusion.

To ensure numerical convergence, the global maximum element size was defined according to the criterion:

$$\Delta x = \frac{c}{10 \cdot f_{\max}} \approx 0.0158\,\text{m} \tag{20}$$

where $c = 1500\,\text{m/s}$ is the speed of sound in water and $f_{\max} = 9500\,\text{Hz}$ is the maximum excitation frequency.

The mesh configuration included the following nodes:

- *Size*: Sets the global element size across the model to define a baseline mesh resolution.
- *Size 1*: Applies local mesh refinement to specific domains or boundaries with expected high gradients in pressure or displacement.
- *Size Expression 1*: Controls element size using a parametric expression, ensuring resolution adapts with frequency and wave properties ($\lambda/10$).
- *Free Triangular 1*: Generates an unstructured triangular mesh adapted to the axisymmetric geometry, particularly useful for capturing complex shapes.
- *Boundary Layers 1*: Adds finely layered mesh elements at the waveguide–water interface to resolve near-field acoustic radiation effects accurately.

The final mesh consisted of 143837 domain elements and 10354 boundary elements, providing a suitable balance between numerical accuracy and computational cost.

A representative meshing configuration is shown in *Figure 6*, which illustrates local refinements in critical structural and acoustic regions. The associated simulation had a total computation time of *8 minutes and 43 seconds*.

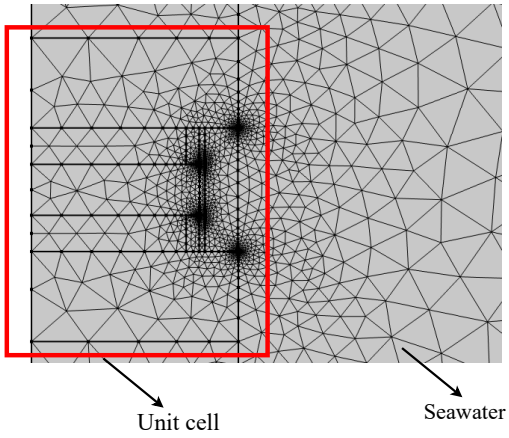

Figure 6: Meshing of the proposed ALWA antenna

F. Study

The type of study employed uses a *Frequency Domain* analysis to model wave propagation phenomena. Assuming harmonic excitation of the pressure field, the time-dependent governing equations can be transformed to the frequency domain, where the time dependence is replaced by the angular frequency parameter $\omega = 2\pi f$. This approach eliminates the explicit time variable, allowing the problem to be solved efficiently using steady-state harmonic formulations. Frequency Domain studies are particularly well suited for simulations involving the finite element or boundary element methods, as implemented in the Acoustics Module. Additionally, this method enables the direct calculation of complex pressure fields, from which amplitude and phase information can be extracted. Important physical effects, such as damping in porous materials and advanced impedance boundary conditions, are inherently accounted for within this framework.

In this work, the simulation is performed over a frequency range from $7800\,\text{Hz}$ to $9500\,\text{Hz}$ with increments of $10\,\text{Hz}$, allowing for detailed analysis of the system's frequency response.

IV. RESULTS AND DISCUSSION

This section presents the numerical results obtained from the simulation of the complete antenna. Specifically, it includes the far-field radiation pattern, directivity, reflection and transmission coefficients, and the radiation efficiency of the system.

A. Radiation Pattern

This represents the distribution of the sound intensity emitted by the antenna in various directions. It is obtained using the boundary conditions and variables related to the far field pressure and the sound pressure level.To compute them, a 1D *Plot Group* of type *Radiation Pattern* is created within the Results section of COMSOL Multiphysics

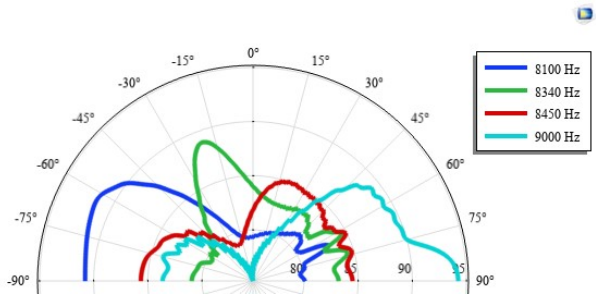

Figure 7: Radiation pattern of the ALWA.

The radiation pattern shown in Fig. 7 illustrates the frequency-dependent beam scanning behavior of the ALWA. The results confirm the dispersive nature of the antenna and its ability to control the radiation angle via frequency tuning.

At $8100\,\mathrm{Hz}$ (blue curve), the main lobe is directed toward negative angles, peaking at approximately $-62°$, with a -3 dB beamwidth of about $88°$, indicating a broad backward radiation pattern with low directivity. At $8340\,\mathrm{Hz}$ (red curve), the beam narrows significantly, reaching a peak at $-20°$ with a beamwidth of $20°$, which reflects increased directivity. At $8450\,\mathrm{Hz}$ (green curve), the main lobe shifts forward, peaking at $+23°$, although the beamwidth expands again to approximately $92°$, revealing a more diffuse radiation pattern. Finally, at $9000\,\mathrm{Hz}$ (black curve), the radiation becomes highly focused, with the main lobe peaking at $+90°$ and a -3 dB beamwidth of $26°$, demonstrating the system's ability to steer acoustic energy by changing frequencies.

These results confirm the ability of the antenna to dynamically steer the acoustic beam by simple frequency tuning. capability of the ALWA and highlight its potential for spatial localization tasks in underwater environments.

B. Directivity

This subsection presents the directivity pattern, which illustrates the sPL as a function of both frequency and radiation angle. The plot provides insight into the angular distribution of radiated acoustic energy across a range of frequencies. This directivity map was generated using COMSOL Multiphysics, which was employed to simulate the acoustic field in the exterior domain of the structure. To compute them, a *1D Plot Group* of type *Directivity*.

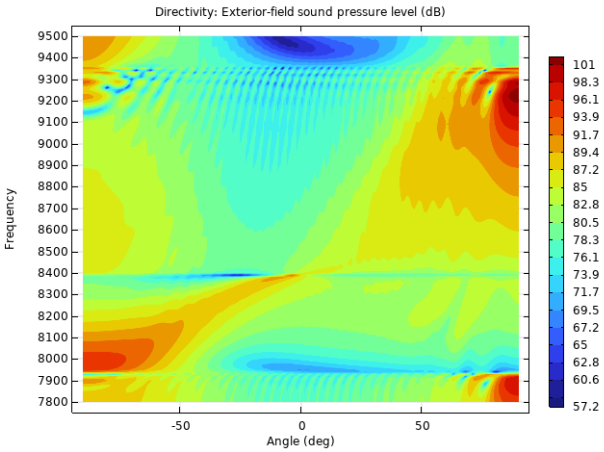

Figure 8: Directivity of the ALWA.

Figure 8 presents the frequency-angle directivity map of the ALWA, where the SPL is plotted in decibels (dB) over a frequency range of $7800\,\mathrm{Hz}$ to $9500\,\mathrm{Hz}$ and an angular range of $-90°$ to $90°$. The color map reveals the angular direction of the main lobe as a function of frequency, a distinctive feature of leaky waveguide behavior. At lower frequencies (e.g., below $8200\,\mathrm{Hz}$), maximum radiation occurs at negative angles, indicating backward radiation. As the frequency increases toward 8340 Hz, the beam transits on the broad side $0°$. Beyond this point, the main lobe is clearly deflected toward positive angles, confirming forward radiation for higher frequencies. The sharp contrast between the high and low acoustic pressure regions demonstrates the antenna's strong directional control and frequency-tuned beam steering. In addition, the interference patterns and sidelobes observed at higher frequencies can be attributed to higher order mode excitations and structural resonances.

C. Reflection and Transmission Parameters and Radiation Efficiency

These parameters provide insight into how the energy of the incident wave is distributed between the reflected and transmitted components. To compute them, a *1D Plot Group* of type *Global* is created within the Results section of COMSOL Multiphysics. In the plot settings, the relevant expressions are defined to evaluate the reflection and transmission behavior of the antenna.

$$|R| = abs(acpr.S11) \tag{21}$$

$$|T| = abs(acpr.S21) \tag{22}$$

$$\eta = 1 - abs(acpr.S11) - abs(acpr.S21) \tag{23}$$

Figure 9 shows the reflection coefficient ($|R|$), transmission coefficient ($|T|$), and radiation efficiency (η_{rad}) of the simulated acoustic leaky wave antenna. In the lower frequency band ($7800\,\text{Hz}$–$8100\,\text{Hz}$), the reflection coefficient exhibits a peak above 0.8, indicating that most of the incident energy is reflected, with minimal transmission and low radiation efficiency. As the frequency increases, the reflection decreases and the transmission coefficient rises, particularly between $8100\,\text{Hz}$ and $8700\,\text{Hz}$, where energy is increasingly transmitted through the structure.

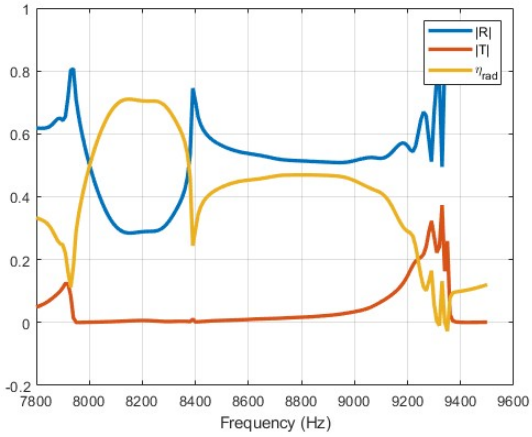

Figure 9: Transmission and reflection parameters and radiation efficiency of the ALWA

Between $8100\,\text{Hz}$ and $8800\,\text{Hz}$, the radiation efficiency also increases, peaking around 0.7. This suggests that a portion of the transmitted energy is effectively radiated into the surrounding fluid. Beyond $9000\,\text{Hz}$, however, both reflection and radiation efficiency exhibit oscillatory behavior, likely due to resonances and structural modal effects, while transmission shows a decreasing trend. The frequency range where $|T|$ and η_{rad} are simultaneously elevated corresponds to effective acoustic radiation, and thus, potential beam steering operation.

Overall, the plot confirms the frequency-dependent behavior of the antenna, with clearly defined bands of transmission, reflection and radiation efficiency characteristic of ALWAs.

V. CONCLUSION

This work has demonstrated the use of COMSOL Multiphysics as a robust and versatile software for the numerical modeling of ALWAs operating in underwater environments. Rather than focusing solely on antenna design, the study emphasizes the capabilities of COMSOL to capture the complex fluid–structure interactions inherent to elastic waveguides coupled with surrounding fluids. By simulating the complete antenna geometry, key indicators such as radiation patterns, reflection and transmission coefficients, directivity and radiation efficiency across a range of frequencies were extracted.

The simulation workflow, including acoustic-structure coupled physics setup, boundary conditions and post-processing strategies, proves to be a reliable framework for frequency-dependent beam steering evaluation and optimization. The results confirm that FEM provides not only quantitative performance predictions, but also valuable physical insight into the radiative behavior of metamaterial-based acoustic devices.

Overall, this study highlights the potential of COMSOL as a powerful tool for the design and analysis of complex acoustic systems, especially where conventional analytical methods are insufficient due to the presence of multiphysics interactions and nontrivial geometries.

REFERENCES

[1] F. Bongard, H. Lissek, and J. R. Mosig, "Acoustic transmission line metamaterial with negative/zero/positive refractive index," *Physical Review B*, vol. 82, no. 9, p. 094306, sep 2010.

[2] C. J. Naify, M. D. Guild, C. A. Rohde, D. C. Calvo, and G. J. Orris, "Demonstration of a directional sonic prism in two dimensions using an

air-acoustic leaky wave antenna," *Applied Physics Letters*, vol. 107, no. 13, sep 2015.

[3] H. Esfahlani, S. Karkar, and H. Lissek, "Optimization of an acoustic leaky-wave antenna based on acoustic metamaterial," Tech. Rep., 2013.

[4] D. R. Jackson, C. Caloz, and T. Itoh, "Leaky-Wave antennas," *Proceedings of the IEEE*, vol. 100, no. 7, pp. 2194–2206, 2012.

[5] A. Fernández-Garrido, M. Campo-Valera, M. E. Abdo-Sánchez, R. Picó, R. Asorey-Cacheda *et al.*, "Diseño de una antena de onda de fuga acústica para la localización espacial." 2024.

[6] F. Monticone and A. Alu, "Leaky-wave theory, techniques, and applications: From microwaves to visible frequencies," *Proceedings of the IEEE*, vol. 103, no. 5, pp. 793–821, 2015.

[7] C. J. Naify, C. N. Layman, T. P. Martin, M. Nicholas, D. C. Calvo, and G. J. Orris, "Experimental realization of a variable index transmission line metamaterial as an acoustic leaky-wave antenna," *Applied Physics Letters*, vol. 102, no. 20, may 2013.

[8] H. Esfahlani, S. Karkar, H. Lissek, and J. R. Mosig, "Exploiting the leaky-wave properties of transmission-line metamaterials for single-microphone direction finding," *The Journal of the Acoustical Society of America*, vol. 139, no. 6, pp. 3259–3266, jun 2016.

[9] S. H. S. Esfahlani, "Electromagnetic inspired acoustic metamaterials: Studying the applications of sound-metastructures interactions based on different wave phenomena," Ph.D. dissertation, Ecole Polytechnique Fédérale de Lausanne, 2017.

[10] A. Fernández-Garrido, M. Campo-Valera, E. Abdo-Sánchez, R. Picó, A.-J. Garcia-Sanchez, and R. Asorey-Cacheda, "Parametric study and experimental validation of acoustic leaky wave antenna in spatial localization," *IEEE Access*, vol. 13, pp. 10 371–10 385, 2025.

[11] I. Felis-Enguix, J. Otero-Vega, M. Campo-Valera, I. Villó-Pérez, and J. Gómez-Tornero, "Practical aspects of acoustic leaky-wave antennas applied to underwater direction finding," *Engineering Proceedings*, vol. 2, no. 1, p. 93, 2020.

[12] C. W. Broadman, C. J. Naify, M. J. Lee, and M. R. Haberman, "Design of a one-dimensional underwater acoustic leaky wave antenna using an elastic metamaterial waveguide," *Journal of Applied Physics*, vol. 129, no. 19, may 2021.

[13] C. Cheng, C. Wang, D. Yang, W. Liu, and F. Zhang, "Underwater localization and mapping based on multi-beam forward looking sonar," *Frontiers in Neurorobotics*, vol. 15, p. 801956, 2022.

[14] A. Fernández-Garrido, M. Campo-Valera, E. Abdo-Sánchez, R. Picó, and R. Asorey-Cacheda, "Modeling of an acoustic leaky-wave antenna for spatial localization," pp. 40–42, 2024, o11.

[15] A. A. Oliner, D. R. Jackson, and J. Volakis, "Leaky-wave antennas," *Antenna engineering handbook*, vol. 4, p. 12, 2007.

[16] C. Caloz and T. Itoh, *Electromagnetic metamaterials: transmission line theory and microwave applications*. John Wiley & Sons, 2005.

[17] COMSOL AB, *COMSOL Multiphysics® 6.3 User Documentation*, COMSOL AB, Stockholm, Sweden, 2025, available online: https://doc.comsol.com/6.3/docserver/#!/com.comsol.help.comsol/helpdesk/helpdesk.html (accessed June 14, 2025).